Shear Alfvén Wave Perpendicular Propagation from the Kinetic to the Inertial Regime

Stephen Vincena,*,† Walter Gekelman, and James Maggs

Department of Physics and Astronomy, University of California at Los Angeles, California, USA
(Received 29 April 2004; published 2 September 2004)

We report on observations of shear Alfvén waves radiated from a source of small transverse size, and the subsequent radial confinement of wave magnetic field energy within a cylindrical plasma. The radius of confinement lies between the kinetic regime of the bulk plasma and the inertial regime at the plasma edge; this radius is found to be a function of wave frequency. Numerical calculations using kinetic theory predict a zero in the perpendicular group velocity at a radius which varies in accord with the observations. An analytic expression for the perpendicular group velocity (valid for small perpendicular wave numbers) is given in the vicinity of the zero crossing.

The magnetized plasmas of stars, planetary magnetospheres, and fusion research are all of finite extent, though their characteristic length scales may be vastly different. This finite nature dictates gradients perpendicular to the background magnetic field in plasma temperature and density. Within these plasmas, slow changes in the magnetic topology are mediated by low-frequency electromagnetic waves such as the shear Alfvén wave. In the ideal, magneto-hydrodynamic (MHD) limit Alfvén waves propagate exactly along the background magnetic field lines, but more realistic descriptions of these waves include the effects of either electron inertia or pressure which leads to a nonzero parallel electric field of the wave and cross-field propagation. This description has been invoked to explain the spatial structure of the shear wave and electron acceleration in phenomena ranging from auroral arcs [1–3], ionospheric density cavities [4,5], coronal loops [6], the solar wind [7], to tokamaks [8] and other laboratory plasmas[9].

When expanding on the MHD limit, it is important to consider the ratio of the electron thermal speed ($v_e^2 = 2T_e/m_e$) to the Alfvén speed ($v_A^2 = B_0^2/4\pi n_i m_i$), where T_e is the electron temperature in eV, m_e the electron mass, B_0 the background field strength, n_i the ion density, and m_i the ion mass. A convenient parameter to distinguish between two limiting regimes is the electron plasma beta $\beta_e = n_e T_e/8\pi B_0^2$, scaled by the ion-to-electron mass ratio: $\bar{\beta}_e \equiv \beta_e m_i/m_e = (v_e/v_A)^2$.

For $\bar{\beta}_e > 1$, the shear wave is termed the "kinetic Alfvén wave"; in this limit, the fast-moving electrons are able to respond adiabatically to the presence of the wave fields. Some authors also use this nomenclature for Alfvén waves with ion Larmor radius effects, but we refer specifically to the $\bar{\beta}_e > 1$ limit. The characteristic perpendicular length scale in this case is the ion sound gyroradius $\rho_s = c_s/\omega_{ci}$, where $c_s = \sqrt{T_e/m_i}$ is the ion sound speed and $\omega_{ci} = eB_0/m_i c$ is the ion-cyclotron frequency, with e the quantum of electric charge and c the speed of light. In the opposite limit ($\bar{\beta}_e < 1$), the inertia of the electrons becomes important, and the shear wave is termed the "inertial Alfvén wave." Here, the characteristic perpendicular length scale is the electron collisionless skin depth $\delta_e = c/\omega_{pe}$, where the electron plasma frequency $\omega_{pe} = \sqrt{4\pi n_e e^2/m_e}$. The kinetic limit is relevant to the physics of the Earth's equatorial magnetosphere and the interior of tokamak plasmas, while the inertial limit applies to the earth's ionosphere and the edge regions of laboratory plasmas.

There is an additional and important distinction between these regimes: for $\bar{\beta}_e > 1$, the wave is forward propagating (with respect to the phase velocity) while for $\bar{\beta}_e < 1$, the wave is backward propagating. This change in sign has been invoked by Streltsov *et al.* [10,11] to explain trapping of dispersive Alfvén waves on auroral magnetic field lines between the ionospheres. Subtle evidence for electron acceleration [12] and wave refraction [13] have been observed in laboratory parallel $\bar{\beta}_e$ gradients. Experiments on Alfvén waves in the intermediate regime have been minimal and mainly limited to measurements of the phase velocity [14,15]. The scarcity of perpendicular group velocity measurements motivates our present investigation.

These experiments are performed in the Large Plasma Device (LaPD) at the University of California, Los Angeles [16]. The device (shown schematically in Fig. 1) is a stainless steel cylindrical vacuum chamber (length = 10 m and diameter = 1 m). Not shown in the figure are the 68 electromagnets surrounding the chamber
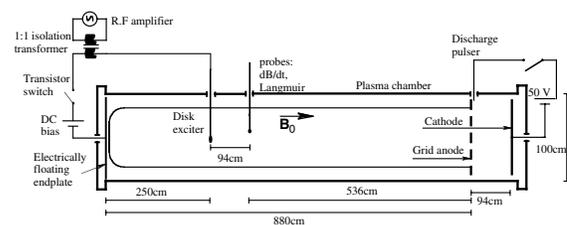

FIG. 1. Schematic of experimental setup.

which produce the confining magnetic field, here at 1.0 kG. The device is backfilled with helium at pressures of approximately 1×10^{-4} torr. The plasma is produced by means of a pulsed ($t = 4.2$ ms, $V = 50$ V) electron discharge between a heated, oxide-coated nickel cathode and a copper mesh anode. The cathode-anode separation is 94 cm, leaving the remainder of the device current free. The highly reproducible discharge is repeated once per second which allows for the collection of ensemble data sets. The wave launching antenna is the same design used in other experiments [9,12,17], and the radiation has been modeled theoretically in both the inertial [18] and kinetic [19] regimes. The antenna is simply a 1 cm diameter, circular copper mesh of 50% optical transparency. It is inserted into the center ($r = 0$) of the plasma column with the normal to the plane of the antenna aligned with the background magnetic field. A positive bias pulse is applied to the antenna for 1.5 ms during the plasma discharge. The antenna bias of 20 V is with respect to a floating copper end plate which terminates the plasma column. The waves are launched by modulating this electron current through an isolation transformer with a 20-cycle, phase-locked tone burst from an rf amplifier at frequencies $\bar{\omega} \equiv \omega/\omega_{ci} < 1$. This method generates shear Alfvén waves with a high degree of azimuthal symmetry [17]. The wave magnetic fields are detected as a function of radius using a 3-axis, differentially wound induction coil probe located a distance $z = 94$ cm from the antenna, and the data are averaged over 20 plasma discharges at each spatial location. The antenna modulation and data acquisition occur 100 μs after the bias is applied, so the $\partial \mathbf{B}/\partial t$ measurements are insensitive to the field produced by the current channel. To first order, the wave magnetic field has only an azimuthal component: $\mathbf{B} \approx B_\theta \hat{\theta}$.

Radial profiles of the electron density (calibrated with a microwave interferometer) and electron temperature are made with a swept Langmuir probe and presented in Fig. 2(a). From these, $\bar{\beta}_e$ is computed and presented in Fig. 2(b). Also shown is an analytic fit which will be used later. The fitting function is arbitrary, but is chosen to reflect features in the data: a flat profile in the bulk plasma and an exponential decay at the plasma edge; it is given by

$$\bar{\beta}_e = \beta_0\{1 - \tanh[(r - r_1)/r_2]\}, \tag{1}$$

with the least-squares fitted parameters: $\beta_0 = 2.0$, $r_1 = 18.4$ cm, and $r_2 = 4.3$ cm.

To discuss the radial propagation of wave energy, it is convenient to consider how much energy is distributed in the wave at any given radius in the plasma. The quantity $\mathcal{U}_\theta$ is defined as the wave magnetic field energy density integrated over the azimuthal coordinate $\mathcal{U}_\theta \equiv \frac{1}{8\pi} \times \int_0^{2\pi}\langle B_\theta\rangle^2 r d\theta$, where $\langle\cdots\rangle$ denotes a sliding, one-period rms-average, centered about the time, t. Using the azimuthal symmetry of the wave patterns, $\mathcal{U}_\theta = r\langle B_\theta\rangle^2/4$. Physically, $\mathcal{U}_\theta \Delta r \Delta z$ yields the magnetic energy of the wave at time, t, in a thin ring; hence, $\mathcal{U}_\theta$ is referred to as
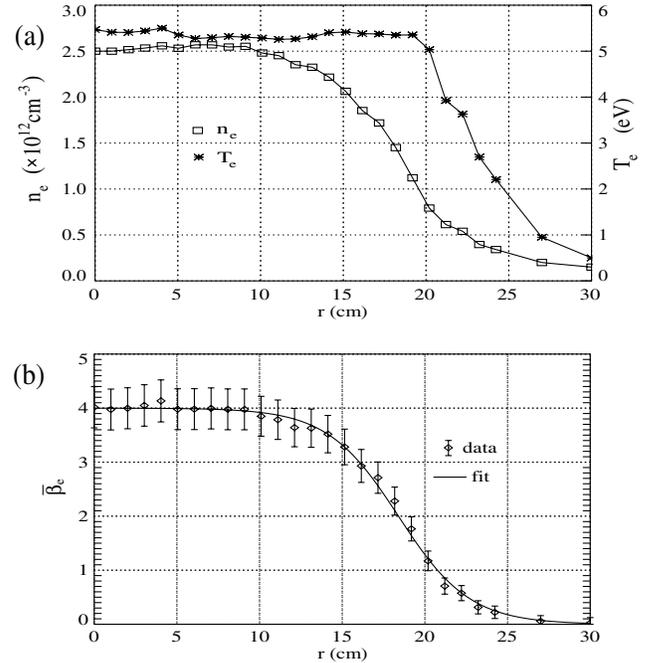

FIG. 2. (a) Measured radial profiles of electron density and temperature. (b) The resulting scaled electron plasma beta, $\bar{\beta}_e = \beta_e m_i/m_e$, along with an analytic fit as described in the text.

the "ring energy density." For large radii, $B_\theta \sim 1/r$ [9,19] and therefore $\mathcal{U}_\theta \sim 1/r$ as well. The wave electric field is of order v_A/c ($\approx 10^{-2}$) smaller than the magnetic field.

Figure 3 presents the time evolution of the ring energy density for $\bar{\omega} = 0.5$ at four select times, with $t = 0$ defined as the initial modulation of the antenna current. The patterns are normalized to their peak value to compare relative features. The pattern after four wave periods is essentially steady state, presumably since the wave has
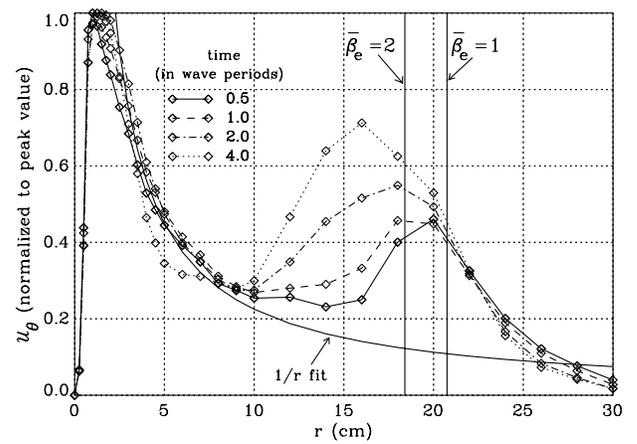

FIG. 3. Time evolution of the radial magnetic field energy density profiles (integrated over the azimuthal coordinate). Error bars (approximately 5% for each value) have been omitted for clarity. The wave frequency is one-half of the ion-cyclotron frequency.

had time to reflect from the axial boundaries. As a function of increasing radius, the patterns for all times shown begin at zero, increase approximately linearly to a peak value, decrease as $1/r$, increase again near the plasma edge, and then decay beyond the point where $\bar{\beta}_e = 1$. The patterns thus comprise two parts: the expected $\mathcal{U}_\theta$ analogous to a current-carrying wire, but where the time-varying currents are those of the Alfvén wave, and a pileup of energy at the plasma edge. The cause of this pileup is interpreted to be the slowing of the perpendicular group velocity: $v_{g\perp}$. Streltsov *et al.* [11] have predicted that for dispersive shear waves, $v_{g\perp}$ should go to zero at $\bar{\beta}_e = 2$ (assuming $T_i = 0$). This point is also shown in Fig. 3, but does not as clearly contain the energy pileup, especially for early times. More importantly, this turning point is not predicted to be a function of frequency, which is discussed next.

Figure 4 shows normalized radial profiles of the ring energy density for two frequencies: $\bar{\omega} = 0.5$ and $\bar{\omega} = 0.9$, centered about the same relative time: one-half period after the initial modulation. To distinguish the energy pileup from the expected $1/r$ behavior, the profiles are modified by fitting and then subtracting a $1/r$ pattern from each. It is clear that the initial deviation from $1/r$ occurs at an increased radius for increased frequency. In addition, the modified profiles are roughly Gaussian in appearance, as evidenced in curves (c) and (d) in Fig. 4. Although there is no *a priori* reason to suspect that the subtracted patterns should have this form, it allows a systematic approach to determine the peak locations. The patterns, however, do not represent probability distributions of a random process, so the standard deviation of the Gaussian fits are not a true measure of the uncer-
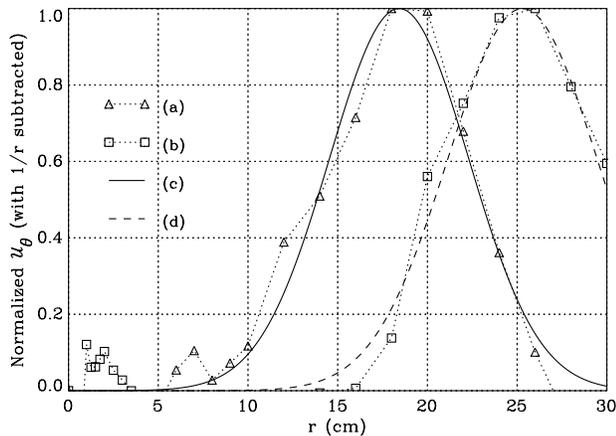

FIG. 4. Frequency variation of the radial magnetic field energy density profiles (integrated over the azimuthal coordinate). The two frequencies shown are (a) $\bar{\omega} = 0.5$ and (b) $\bar{\omega} = 0.9$. For both frequencies, a $1/r$ profile is fit to the data, subtracted, and that result is fit to a Gaussian, shown in curves (c) and (d). For small radii, the wave pattern does not behave as $1/r$ and the subtraction results in large negative numbers, which are not plotted.

tainty of the peak location; instead, the uncertainty is taken to be equal to the radial step size ($\Delta r = 2$ cm for $r > 10$ cm). In the remainder of this section, a theoretical explanation for the frequency dependence is developed and compared to the data.

In cylindrical geometry, the dispersion relation for shear Alfvén waves may be written in terms of the elements of the dielectric tensor $\boldsymbol{\epsilon}$ and the index of refraction $\mathbf{n} = c\mathbf{k}/\omega$, as

$$n_\perp^2 \epsilon_\perp + n_\parallel^2 \epsilon_\parallel = \epsilon_\perp \epsilon_\parallel, \tag{2}$$

where $\perp$ ($\parallel$) indicates the component perpendicular (parallel) to $\mathbf{B}_0$. From this, the perpendicular group velocity is given by

$$v_{g\perp} = 2k_\perp \left[\left(\frac{\omega^2}{c^2} - \frac{k_\parallel^2}{\epsilon_\perp} \right) \frac{\partial \epsilon_\parallel}{\partial \omega} + \epsilon_\parallel \left(\frac{2\omega}{c^2} + \frac{k_\parallel^2}{\epsilon_\perp^2} \frac{\partial \epsilon_\perp}{\partial \omega} \right) \right]^{-1}. \tag{3}$$

This expression is general and can be used numerically for a wide range of parameters; however, a simplified expression may be obtained for experimental conditions in the LaPD. First, T_i is set equal to zero. This approximation is valid in the LaPD for frequencies as high as $\bar{\omega} = 0.95$ [12]; however, it cannot necessarily be made for plasmas such as the Earth's equatorial magnetosphere or those within the interiors of tokamaks. Also, the plasma is assumed to be collisionless, so that the only damping of wave energy will be through electron Landau damping. Finally, terms higher than first order in $k_\perp L$ are ignored, where L is either of the length scales: ρ_s or δ_e.

The perpendicular dielectric tensor element (given by Stix [20]) is $\epsilon_\perp = (c/v_A)^2/(1 - \bar{\omega}^2)$, and the parallel element is $\epsilon_\parallel = -(\omega_{pe}/\omega)^2 \zeta^2 Z'(\zeta)$, where ζ is the ratio of the parallel wave phase speed to the electron thermal speed ($\zeta \equiv \omega/k_\parallel v_e$) and Z' is the derivative of the plasma dispersion function [21] with respect to its argument. With these assumptions, $k_\parallel^2 = \omega^2 v_A^{-2}(1 - \bar{\omega}^2)^{-1}$, and Eq. (3) reduces to

$$v_{g\perp} = -2k_\perp \rho_s^2 \omega / Z'(\zeta). \tag{4}$$

Two limiting forms of this expression are easily obtained: in the kinetic limit, $Z' \to -2$ and $v_{g\perp} = k_\perp \rho_s^2 \omega$; while in the inertial limit, $Z' \to \zeta^{-2}$ and $v_{g\perp} = k_\perp \delta_e^2 \omega (1 - \bar{\omega}^2)$. These are the correct expressions [18,19] for the above assumptions.

In general, Z' and hence $v_{g\perp}$ will be complex-valued functions and we interpret the real part as being the physically measurable quantity. Stratton [22] offers a discussion of wave packet propagation in a dispersive and dissipative medium. With this interpretation,

$$v_{g\perp} = -2k_\perp \rho_s^2 \omega \operatorname{Re}[Z'(\zeta)]/|Z'(\zeta)|^2. \tag{5}$$

Note that $v_{g\perp}$ goes to zero when the real part of Z' does. With an assumption of weak damping, ζ is approximately a real number (denoted by ζ_R) and $\operatorname{Re}[Z'(\zeta_R)] = 0$ at
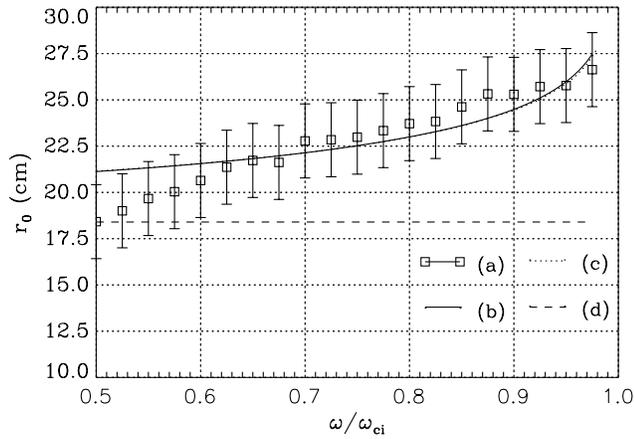
FIG. 5. Radial location of zero perpendicular group velocity as a function of frequency. Shown are (a) measured locations determined from Gaussian fits to the wave energy pileup, (b) predictions using the simplified expression of Eq. (6), (c) predictions of Eq. (3) [this nearly overlaps (b)], and (d) predictions using the theory of Streltsov *et al.* [11] with $T_i = 0$.

$\zeta_R = \pm\zeta_0$, where $\zeta_0 \approx 0.924$. The two values of ζ_R are for waves traveling in the $\pm z$ directions. In either case, $\zeta^2 = (1 - \bar{\omega}^2)/\bar{\beta}_e$ and the radius at which $v_{g\perp} = 0$, denoted r_0, is determined through the relation $\bar{\beta}_e(r = r_0) = (1 - \bar{\omega}^2)/\zeta_0^2$. Using Eq. (1),

$$r_0 = r_1 + r_2 \tanh^{-1}\left[1 - (1 - \bar{\omega}^2)/(\beta_0\zeta_0^2) \right]. \qquad (6)$$

Figure 5 displays the experimental values of r_0 obtained from Gaussian fits of $\mathcal{U}_\theta$, as in Fig. 4, and [as curve (b)] the result of Eq. (6). Also included in this figure [curve (c)] are the values of r_0 obtained from the zero crossing predicted by taking the real part of a numerical calculation of Eq. (3) using local solutions of the dispersion relation, Eq. (2), and assuming a fixed value of $k_\perp = 0.35$ cm^{-1}. Note from Eq. (5) that the zero crossing itself will be independent of $k_\perp$. The two curves (b) and (c) are nearly indistinguishable, which justifies the assumptions used to obtain Eq. (4). Also shown in Fig. 5 is the frequency-independent prediction of Streltsov *et al.*[11]. Although the zero of the group velocity is not directly measured, there is a general agreement as a function of frequency between the predictions of Eq. (6) and the initial deviation of $\mathcal{U}_\theta$ from a $1/r$ pattern. The results are not as good at low frequencies, which could be the result of a near field effect of the antenna because the parallel wavelengths are longer at lower frequencies.

In summary, we have provided the first (to our knowledge) clear experimental evidence for the theoretically predicted perpendicular group velocity turning point between the kinetic and inertial regimes of the shear Alfvén wave. The turning point is a function of frequency as predicted by the kinetic dispersion relation. Although the wave amplitudes in this experiment were too small to significantly heat the plasma, the transition from large to small $\bar{\beta}_e$ is an effective way to confine Alfvén wave energy and to create localized regions of electron acceleration via Landau damping of the wave.

*Electronic address: vincena@physics.ucla.edu
†URL: http://plasma.physics.ucla.edu
[1] D. W. Swift, J. Geophys. Res. **80**, 2096 (1975).
[2] A. Hasegawa, J. Geophys. Res. **81**, 5083 (1976).
[3] C. K. Goertz, Planet. Space Sci. **32**, 1387 (1984).
[4] P. Louarn, J. E. Wahlund, T. Chust, H. de Feraudy, A. Roux, B. Holback, P. O. Dovner, A. I. Eriksson, and G. Holmgren, Geophys. Res. Lett. **21**, 1847 (1994).
[5] V. Génot, P. Louarn, and D. L. Quéau, J. Geophys. Res. **104**, 22649 (1999).
[6] D. J. Wu and C. Fang, Astrophys. J. **511**, 958 (1999).
[7] R. J. Leamon, C. W. Smith, N. F. Ness, and H. K. Wong, J. Geophys. Res. **104**, 22331 (1999).
[8] N. I. Grishanov, G. O. Ludwig, C. A. de Azevedo, and J. P. Neto, Phys. Plasmas **9**, 4089 (2002).
[9] W. Gekelman, D. Leneman, J. Maggs, and S. Vincena, Phys. Plasmas **1**, 3775 (1994).
[10] A. Streltsov and W. Lotko, J. Geophys. Res. **100**, 19457 (1995).
[11] A. V. Streltsov, W. Lotko, J. R. Johnson, and C. Z. Cheng, J. Geophys. Res. **103**, 26559 (1998).
[12] S. Vincena, W. Gekelman, and J. Maggs, Phys. Plasmas **8**, 3884 (2001).
[13] C. C. Mitchell, J. E. Maggs, S. T. Vincena, and W. N. Gekelman, J. Geophys. Res. **107**, SMP28-1 (2002).
[14] D. Leneman, W. Gekelman, and J. Maggs, Phys. Rev. Lett. **82**, 2673 (1999).
[15] C. A. Kletzing, S. R. Bounds, J. Martin-Hiner, W. Gekelman, and C. Mitchell, Phys. Rev. Lett. **90**, 035004/1 (2003).
[16] W. Gekelman, H. Pfister, Z. Lucky, J. Bamber, D. Leneman, and J. Maggs, Rev. Sci. Instrum. **62**, 2875 (1991).
[17] W. Gekelman, S. Vincena, D. Leneman, and J. Maggs, J. Geophys. Res. **102**, 7225 (1997).
[18] G. J. Morales, R. S. Loritsch, and J. E. Maggs, Phys. Plasmas **1**, 3765 (1994).
[19] G. J. Morales and J. E. Maggs, Phys. Plasmas **4**, 4118 (1997).
[20] T. H. Stix, *Waves in Plasmas* (McGraw-Hill, New York, 1992).
[21] B. D. Fried and S. D. Conte, *The Plasma Dispersion Function* (Academic Press, Inc., New York, 1961).
[22] J. A. Stratton, *Electromagnetic Theory* (McGraw-Hill, New York, 1941).